



# Extraction of vibration waveform characteristics of dry ice powder pneumatic rock breaking using Hilbert-Huang transform

Xiaofei Wang<sup>1,2,3,4</sup> · Shaobin Hu<sup>5,6,7</sup> · Enyuan Wang<sup>1,2,3,4,8</sup> · Qiang Zhang<sup>9</sup> · Bing Liu<sup>1,2,3,4</sup>

Received: 1 September 2021 / Accepted: 4 December 2021 / Published online: 29 December 2021  
© Saudi Society for Geosciences 2021

## Abstract

In order to promote the development of the new dry ice powder pneumatic rock breaking technology and the safety and environmental pollution assessment of the application site, this paper measures the vibration and noise generated by the dry ice powder pneumatic rock breaking process and extracts the vibration through the Hilbert-Huang transform analysis method. The test results show that (1) the noise measurement found that the noise propagation is directional. The pre-splitting of the first shot makes the second shot of the noise spread more quickly and the sound pressure level is higher. (2) Compared with the Fourier transform, HHT transform is a better tool to extract the characteristics of vibration waveform. (3) When the focal distance is 7 m, the distribution of energy in frequency is scattered, and the damage of vibration to buildings can be considered more comprehensively through the distribution of energy in time and frequency.

**Keywords** Hilbert-Huang transform (HHT) · Dry ice powder pneumatic rock breaking · Noise measurement · Vibration waveform

## Introduction

Rock breaking work is often required in engineering construction. Drilling and blasting has become the most commonly used rock breaking method due to its high efficiency and huge scale (DOBRATZ et al. 1985; SANCHIDRIÁN 2018; Haugen 2018). However, with the progress of society, explosives have a high risk factor, construction approval is difficult, destructive, and the shortcomings of easily causing air pollution have become more and more obvious (Global

1995; Roy et al. 2020; Singh et al. 2020; Zhou et al. 2020; Hu and Lu 2018). At the same time, the explosion shock wave generated by drilling and blasting may affect the surrounding buildings and residents, causing serious noise pollution and not meeting the requirements of green construction. Therefore, drilling and blasting rock is more and more strictly controlled, and the application field is getting smaller and smaller (Zhang et al. 2018; Mondal Debjeet and Roy 2019). CO<sub>2</sub> is a kind of gas that is easy to compress and liquefy. At room temperature, liquid CO<sub>2</sub> is transformed into gas, and its volume becomes 600 times its original volume,

Responsible Editor: Longjun Dong

✉ Shaobin Hu  
hsbhhu@126.com

✉ Enyuan Wang  
weytop@cumt.edu.cn

<sup>1</sup> Key Laboratory of Gas and Fire Control for Coal Mines, China University of Mining and Technology, Ministry of Education, Xuzhou 221116, Jiangsu, China

<sup>2</sup> National Engineering Research Center for Coal Gas Control, China University of Mining and Technology, Xuzhou 221116, Jiangsu, China

<sup>3</sup> State Key Laboratory of Coal Resources and Safe Mining, China University of Mining and Technology, Xuzhou 221116, Jiangsu, China

<sup>4</sup> School of Safety Engineering, China University of Mining and Technology, Xuzhou 221116, Jiangsu, China

<sup>5</sup> Key Laboratory of Ministry of Education for Geomechanics and Embankment Engineering, HoHai University, Nanjing 210098, Jiangsu, China

<sup>6</sup> Tunnel and Underground Engineering Institute, College of Civil and Transportation Engineering, HoHai University, Nanjing 210098, Jiangsu, China

<sup>7</sup> HoHai University, Nanjing 210098, Jiangsu, China

<sup>8</sup> China University of Mining and Technology, Xuzhou 221116, Jiangsu, China

<sup>9</sup> ChinaPower China Huadong Engineering Corporation Limited, Hangzhou 311122, Zhejiang, China

causing strong physical expansion to break the rock formation and achieve the effect of replacing explosives. Liquid CO<sub>2</sub> phase change rock fragmentation technology has attracted wide attention in the field of rock excavation due to its advantages of low noise, environmental protection, low risk factor, and small vibration impact on surrounding buildings and residents (Chen et al. 2017; Gao et al. 2018; Yang et al. 2020; Song and Chen 2020; Zhang and Chen 2020; Ebrahim and Ewan 2021; Feng and Lu 2021). The concept of liquid CO<sub>2</sub> phase change fracturing was first proposed by the British Cardox company in the 1950s, and rock fracturing was achieved through CO<sub>2</sub> fracturing tubes (Donze et al. 1997). Its main working process is to heat the liquid CO<sub>2</sub> by heating the agent to make it absorb heat and expand, and through the rupture of the CO<sub>2</sub> fracturing tube, release the high-energy CO<sub>2</sub> fluid in the supercritical state to achieve the rupture of the rock. At present, this technology is mainly used in coal fracturing to increase the efficiency of coalbed methane extraction. Many scholars at home and abroad have carried out extensive research on this technology (Kutter and Fairhurst 1971; Nilson et al. 1985; Zhang et al. 2019; Goodarzi et al. 2015; Xie et al. 2018; Liu et al. 2018; Li et al. 2018; Li et al. 2020). However, the traditional repetitive CO<sub>2</sub> cracker is prone to flying tube accidents when detonating; the disposable CO<sub>2</sub> cracker is prone to abnormal tube explosion accidents due to the direct formation of great lethality during the blasting process. Aiming at the potential safety hazards of traditional liquid CO<sub>2</sub> phase change fracturing technology, Hu et al. (2019) proposed a new type of dry ice powder pneumatic fracturing and rock breaking technology, which mainly uses the large amount of heat released by the combustion of intrinsically safe CO<sub>2</sub> accumulators under voltage excitation. Pneumatic rock breaking is realized by phase change of dry ice powder.

Whether it is rock drilling and blasting or dry ice powder pneumatic rock breaking technology, during the rock breaking process, a part of the energy is converted into seismic energy and dissipated, causing vibrations on the ground near the rock breaking area. It is the main cause of damage to buildings or other infrastructure in the area near the broken rock (Kumar and Mishra 2020). The vibration signal generated during the blasting process can be collected by the microseismic monitoring system (Yang et al. 2008). Vibration analysis is an extremely important topic. There are many methods for simulating ground vibrations, such as the method based on the source model convolution Green's functions (e.g., Ma et al 2018; Ma et al 2019), spectral element methods (e.g., Wang and Cai 2017; Dhanya et al 2017), and empirical function methods (e.g., Kaveh et al. 2016). In order to obtain the signal characteristics of the microseismic signal, some time–frequency analysis techniques need to be used. The fast Fourier transform (FFT) time–frequency analysis method is

convenient and fast and has been widely used in the field of signal analysis (Song et al. 2015; Lu et al. 2012; Chernov and Sokolov 1999). However, FFT requires the signal to have quasi-periodicity and stability (Benson et al. 2010; Lu et al. 2013; He et al. 2010). Therefore, FFT is not suitable for the analysis of nonlinear signals (Cohen and Bai 1998; Chaparro 2015). In view of the deficiencies of FFT, wavelet analysis proposed by French geophysicists can extract depth information from nonlinear signals (Morlet 1982). The wavelet method is one of the best available techniques for analyzing nonlinear signals and is often used in image processing, speech analysis, pattern recognition, quantum physics, and seismic waveforms (Rachel and Willsky 1995; Mallat 1989; Chui 1992). However, wavelet transform is only a FFT with adjustable window, which is limited by Heisenberg's uncertainty principle. At the same time, the choice of adjustable window of wavelet transform is greatly influenced by subjective factors, which is not conducive to the objective extraction of signal features (Babu et al. 2008). The Hilbert-Huang transform (HHT) analysis method consists of empirical mode decomposition (EMD) and Hilbert-Huang transform (HT). EMD can objectively process nonlinear signals and provide accurate time resolution for the energy–frequency representation of the signal, overcoming the shortcomings of wavelet analysis (Wu and Huang 2004). HHT signal analysis technology has been widely used in various fields, such as biomedicine, finance, and geology (Skeberis et al. 2015; Elgamel and Soraghan 2011; Li et al. 2016a, b).

When the traditional repetitive CO<sub>2</sub> cracker is detonated, it is easy to fly and it is very dangerous; because the disposable CO<sub>2</sub> cracker directly forms great lethality during the blasting process; it is prone to bursting. In view of the hidden safety hazards of traditional CO<sub>2</sub> phase change expansion fracturing technology, Hu et al (2019) proposed a new type of dry ice powder pneumatic fracturing process, which mainly uses the intrinsically safe CO<sub>2</sub> accumulator with independent intellectual property rights to burn and release under voltage excitation. At present, there is a lack of research on the vibration signal characteristics of dry ice pneumatic rock breaking technology, which is not conducive to the safety research and promotion of new rock breaking technology. In this paper, a field test of a new type of dry ice pneumatic rock breaking technology is carried out in an ore factory. The vibration and noise signals generated by blasting are measured. HHT has advantages in the feature extraction of blasting vibration signals. The HHT method is used to analyze the vibration waveform signals caused by dry ice powder pneumatic rock breaking feature. The research results have an important guiding role in the field engineering practice and safety environmental assessment of dry ice powder pneumatic fracturing technology.

## Field test

### Experimental location and rock breaking process

#### 1. Experimental location

As shown in Fig. 1, the test site is selected at Jinxin Ore Factory, Shihe Town, Dazhu County, Dazhou City, Sichuan Province. The main lithology of the ore factory is tuff, and the main physical properties are shown in Table 1. Ore plants currently mainly use drilling and blasting rocks, causing noise pollution and harmful gas pollution. In order to reduce pollution and ensure the efficiency of rock breaking, and to consider the impact on the adjacent area, a dry ice powder pneumatic rock breaking test was carried out in this area. The microseismic monitoring system and noise monitoring system were used to monitor the rock breaking process throughout the whole process, and the vibration and noise waveforms of the rock breaking process were obtained.

#### 2. Rock breaking equipment and rock breaking process

The rock-breaking equipment uses the L-600 dry ice cracker produced by Jiangsu Zhongkong Energy Technology Co., Ltd., as shown in Fig. 2. This type of cracker is 600 mm in length and 90 mm in diameter. It is mainly composed of dry ice powder cabin, heating rod, CO<sub>2</sub> accumulator,

**Table 1** Physical and mechanical properties of the specimens

Density/g/cm <sup>3</sup>	Uniaxial compressive strength/MPa	Elastic modulus/GPa	Poisson's ratio
2.73	100.02	21.55	0.13

detonator, heating wire, detonating wire, and safety conduit. The dry ice powder cabin is used to hold dry ice powder, the detonator is used to ignite the CO<sub>2</sub>-EA, and the CO<sub>2</sub>-EA is used to quickly burn to provide heat. The safety pipe can be connected to an external pressure sensor to measure the pressure and deflate when the detonation is unsuccessful. The CO<sub>2</sub> accumulator used is a porous micro-nano structured functional material with strong adsorption characteristics, and this structure is conducive to the combustion exothermic reaction of the CO<sub>2</sub> accumulator. The physical and chemical parameters of the accumulator are shown in Tables 2

The essence of dry ice powder pneumatic rock breaking technology is that the dry ice phase changes into liquid CO<sub>2</sub> after being heated. After activating the detonator, the accumulator is ignited and burns quickly. The CO<sub>2</sub> in the dry ice compartment is heated quickly, and the temperature and pressure rises and finally reaches the breaking pressure. The rupture tube ruptured. After the cracking tube ruptures, a large

**Fig. 1** Test site

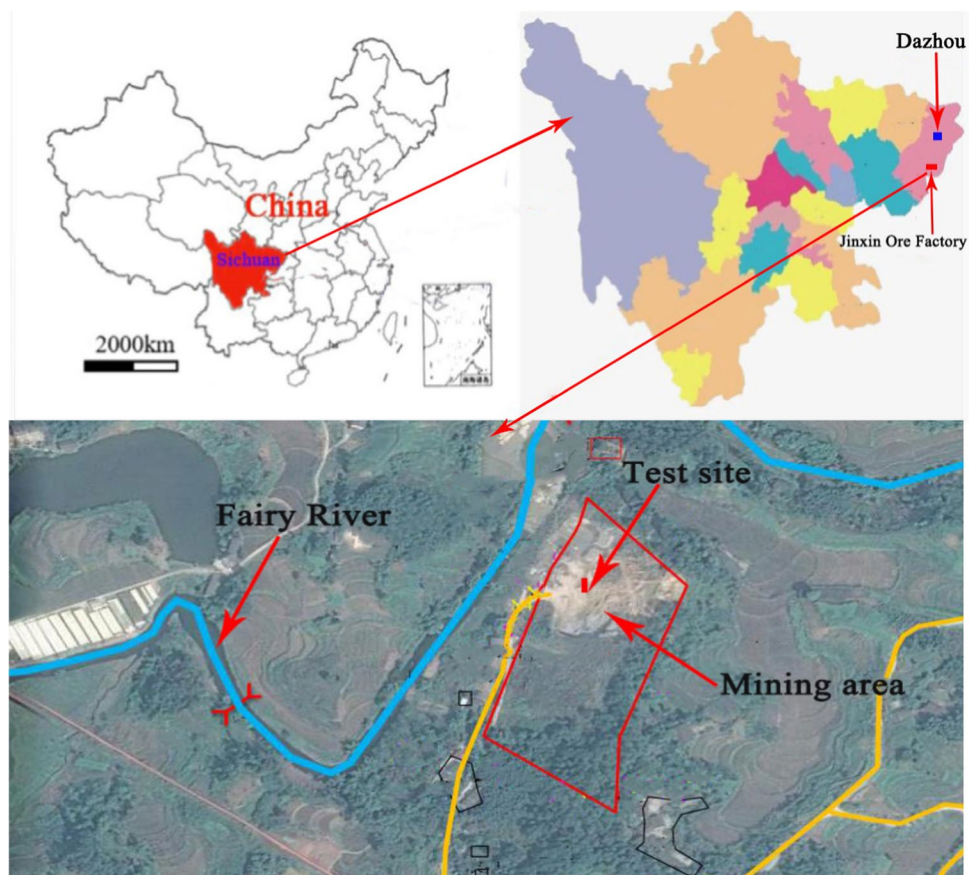


**Fig. 2** Structure diagram of L-600 dry ice powder cracker (a dry ice powder cabin, b heating rod, c CO<sub>2</sub>-EA d detonator, e heating wire, f detonating wire, g safety conduit)

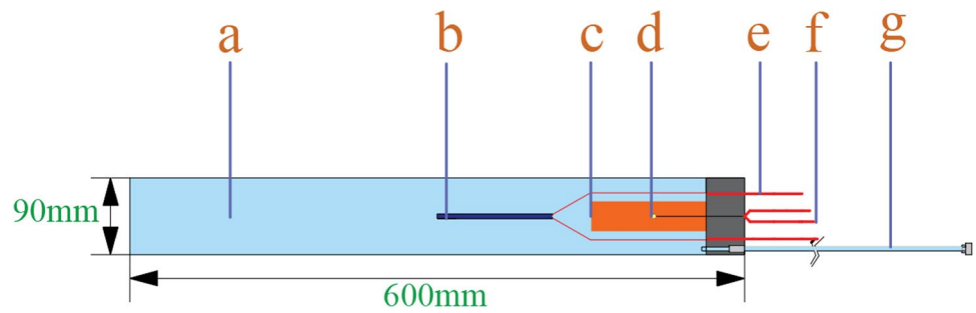


**Table 2** Basic physical and chemical parameters of the CO<sub>2</sub>-EA [21]

Material	Apparent density (g/mL)	Porosity	Specific surface area (m <sup>2</sup> /g)	Heat of combustion (kJ/g)	Thermal conductivity (W/m k)
CO <sub>2</sub> -EA	0.12	0.92	240	21.33	0.016

**Table 3** Noise sound pressure level test results

Sensor number	N1	N2	N3
SPL1 (dB)	101.57	98.21	90.06
SPL2 (dB)	111.65	114.75	107.35

amount of gas is released and impacts and compresses the surrounding rock medium, causing rock damage in the nearby area and completing the rock breaking work. At the site, we used a pressure sensor to connect with the safety valve, and the measured burst critical pressure was 53.60 MPa.

Before breaking the rock, drill holes were required. The diameter was 110 mm, the depth was 1.5 m, and the angle with the ground was 40 degrees. A total of 6 holes were drilled, and three dry ice cracking tests were carried out. After the drilling is completed, a cracker is installed in the borehole, the hole is sealed with a sealing material, and the length of the hole is 0.9 m and use an electric detonator to excite the accumulator. Among them, the mass of dry ice powder used in a single fracturing tube is 1.5 kg, and the resistance wire heating wire has been prefabricated in the CO<sub>2</sub> accumulator tube in advance.

### Vibration and noise monitoring and measuring point layout

#### 1. System introduction

The test equipment is composed of a collector, an acceleration sensor, an acoustic sensor, and a computer and records the original time domain signals of vibration and noise before and after rock breaking. The acquisition instrument is a network

distributed 16-channel acquisition instrument INV 3062S/V prepared by Beijing Oriental Noise and Vibration Research Institute. The acceleration sensor is a general piezoelectric acceleration sensor INV9828, and the acoustic sensor is a high-precision IEPE sound pressure sensor INV9206.

#### 2. Layout of measuring points

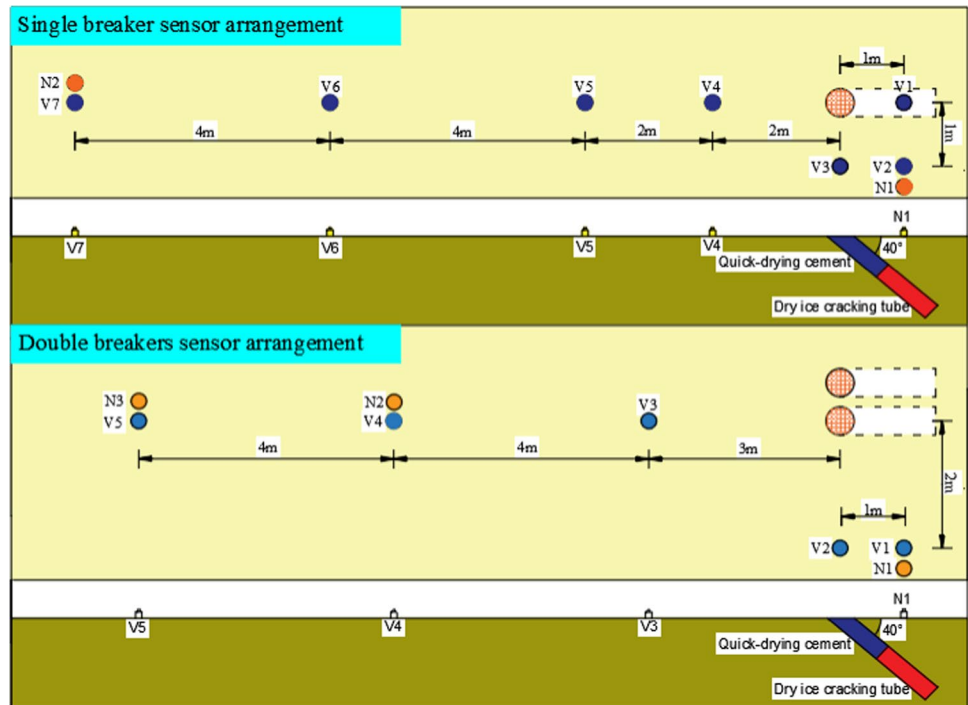
The vibration sensor layout network is shown in Fig. 3. A total of 7 vibration sensors and two noise sensors are arranged for a single fracturing tube rock breaking experiment. V1 is placed directly above the borehole, V2 is placed 1 m to the right of V1, V3 is placed 1 m to the right of the borehole, and V4, V5, V6, and V7 are placed in sequence along the front of the borehole. The noise sensors N1 and N2 are respectively arranged beside V2 and V7. A total of 5 vibration sensors and 3 noise sensors were arranged in the rock breaking experiment of the two fracturing tubes. V1 is arranged at a position 2 m on the right side of the borehole, and the horizontal distance from the borehole opening is 1 m; V2 is arranged at a position 2 m on the right side of the borehole opening, and V3, V4, and V5 are arranged in sequence along the front of the borehole. The noise sensors N1, N2, and N3 are respectively arranged beside V1, V4, and V5. Figure 3 shows the schematic diagram of rock breaking location and sensor layout. In order to fully couple the vibration sensor with the ground, it was fixed with a mixture of gypsum powder and water, and the test was performed after the gypsum was hardened. The noise sensor is fixed at a distance of 1.5 m from the ground with a bracket, and a sponge head is used to filter the influence of other sound sources.

### Test results

#### Noise measurement and sound pressure level calculation

As shown in Fig. 4, for the field test noise waveforms, N1, N2, and N3 are respectively arranged at 2 m, 7 m, and 11 m away from the seismic source. The two dry ice fracturing tube excitations produced obvious nonlinear waveforms. The pressure peaks are N1: P<sub>m1</sub> = 2.396 Pa, P<sub>m2</sub> = 7.647 Pa; N2: P<sub>m1</sub> = 1.628 Pa, P<sub>m2</sub> = 10.922 Pa; N3: P<sub>m1</sub> = 0.637 Pa,

**Fig. 3** Schematic diagram of sensor and dry ice fracturing tube layout



$P_{m2} = 4.663$  Pa, the measured data is pressure data, through the calculation formula of sound pressure level:

$$SPL = 201g \left[ \frac{P_{(e)}}{P_{(ref)}} \right] \tag{1}$$

In the formula: SPL is the sound pressure level in dB,  $P_{(e)}$  is the measured pressure in pa,  $P_{(ref)}$  is the reference sound pressure in the air, generally  $2 \times 10^{-5}$  pa. The noise test results can be calculated as shown in the Table 3: N1 is only 2m away from the explosion point, and the noise sound pressure levels of the first and second dry ice powder cracking tubes after detonation are only 101.57 dB and 111.65 dB. As the distance increases, the noise sound pressure level decreases slowly. N3 is 11 m away from the burst point. The first shot caused the noise sound pressure level to 90.06 dB, and the second shot caused the noise sound pressure level to 107.35 dB. At the same time, the noise sound pressure levels in different directions are not the same. N1 is located on the right side of the explosion point, and both N2 and N3 are located directly in front of the explosion point. The noise caused by the excitation of the second dry ice powder cracking tube is greater in the front because even if N2 is farther away from the explosion point, the noise sound pressure level caused by the second shot is greater than the value measured at N1.

**Vibration waveform induced by dry ice powder pneumatic rock breaking**

Figure 5 shows the vibration waveform measured after the double-head dry ice fracturing tube is excited. The test data of V1 is

affected by the vibration due to the too close distance. Two obvious waveform changes can be found through observation. The two fracturing tubes are excited in sequence, and the second vibration peak and noise peak are both larger from the peak value. Observed from the results of the V5 waveform, when the source distance reaches 11 m, the vibration speed is below 25 mm/s, which meets the safety requirements of building vibration and is far lower than the vibration intensity of drilling and blasting construction.

**FFT to analyze the frequency spectrum**

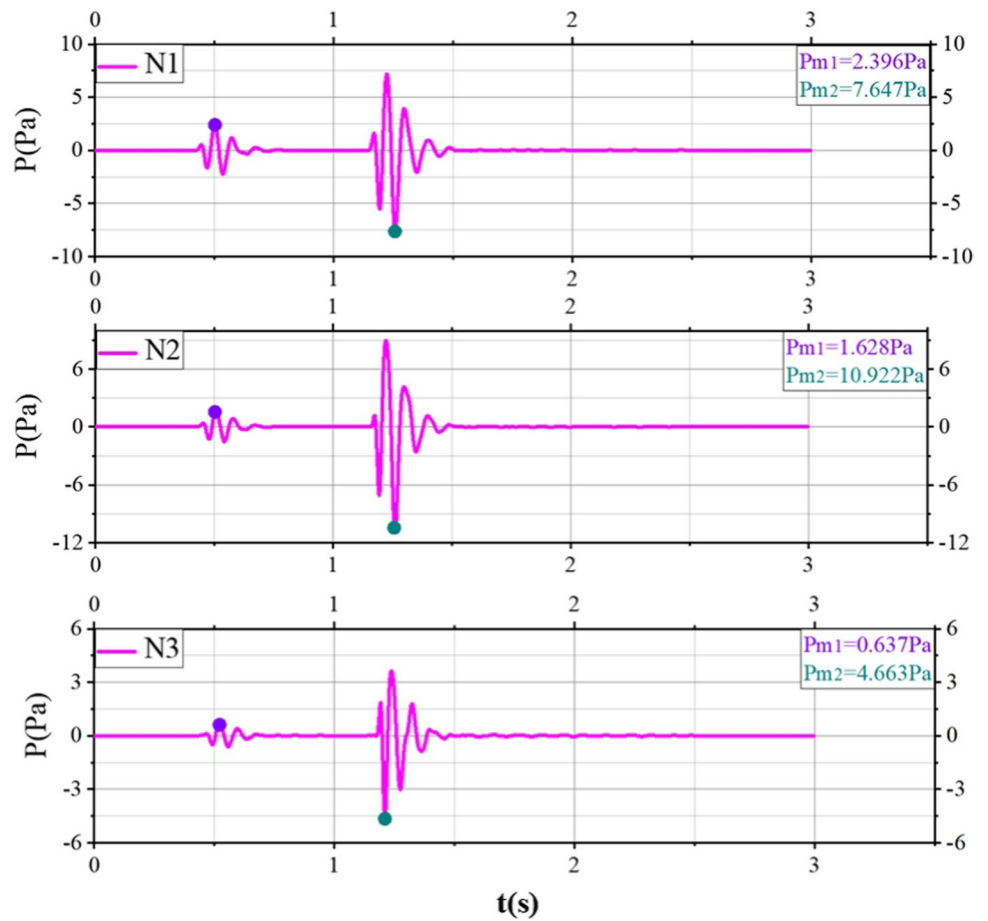
As shown in Fig. 6, all the waveforms are processed by fast Fourier transform to obtain a Fourier spectrogram. The fast Fourier transform transforms the signal from the time domain to the frequency domain, which provides a very convenient and effective method for processing vibration waveforms. As the focal distance increases, high-frequency signals decay faster than low-frequency signals, and signals above 20 Hz decay faster than 10–20 Hz. As the focal distance increases, the amplitude of the high- and low-frequency signals decreases rapidly, which is consistent with the rapid decrease of the peak wave velocity.

**Hilbert-Huang transform of vibration waveform**

**Introduction to Hilbert-Huang Transform**

The main content of HHT consists of two parts. The first part is empirical mode decomposition (EMD), which is proposed by

**Fig. 4** Waveform of noise measurement



Huang; the second part is Hilbert spectrum analysis (HSA). To put it simply, the basic process of HHT processing non-stationary signals is first, use the EMD method to decompose a given signal into a number of intrinsic mode functions (represented by intrinsic mode function or IMF, also known as intrinsic mode functions). IMF is a component that meets certain conditions; then, the Hilbert transform is performed on each IMF to obtain the corresponding Hilbert spectrum, that is, each IMF is represented in the joint time–frequency domain; finally, the Hilbert spectrum of all IMFs will be summed to get the original signal Hilbert spectrum. The EMD process can be summarized as follows:

1. Initialization:  $r_0 = x(t)$ ,  $i = 1$ .
2. Extract the first IMF.
  - a. Initialization:  $h_{i(k-1)} = r_i$ ,  $k = 1$ .
  - b. Extract  $h_{i(k-1)}$ .
  - c. Use cubic splines to interpolate local extremums and minimums to form  $h_{i(k-1)}$ .
  - d. Calculate the mean  $m_{i(k-1)}$  of the upper and lower envelopes of  $h_{i(k-1)}$ .
  - e. Let  $h_{ik} = h_{i(k-1)} - m_{i(k-1)}$ .
  - f. If the stop criterion is met, set  $IMF_i = h_{ik}$ , otherwise go to step (b) and set  $k = k + 1$ .

3. Define  $r_{i+1} = r_i - IMF_i$ .

If  $r_{i+1}$  still has at least 2 extreme values, go to step (2); otherwise, the decomposition process ends, and  $r_{i+1}$  is the remainder of the signal. Secondly, perform Hilbert transform for each IMF, and according to

$$a(t) = [x^2(t) + y^2(t)]^{1/2}, \varphi(t) = \arctan(y(t)/x(t)), \omega(t) = \frac{d\varphi(t)}{dt} \tag{2}$$

Calculate the instantaneous frequency and amplitude.

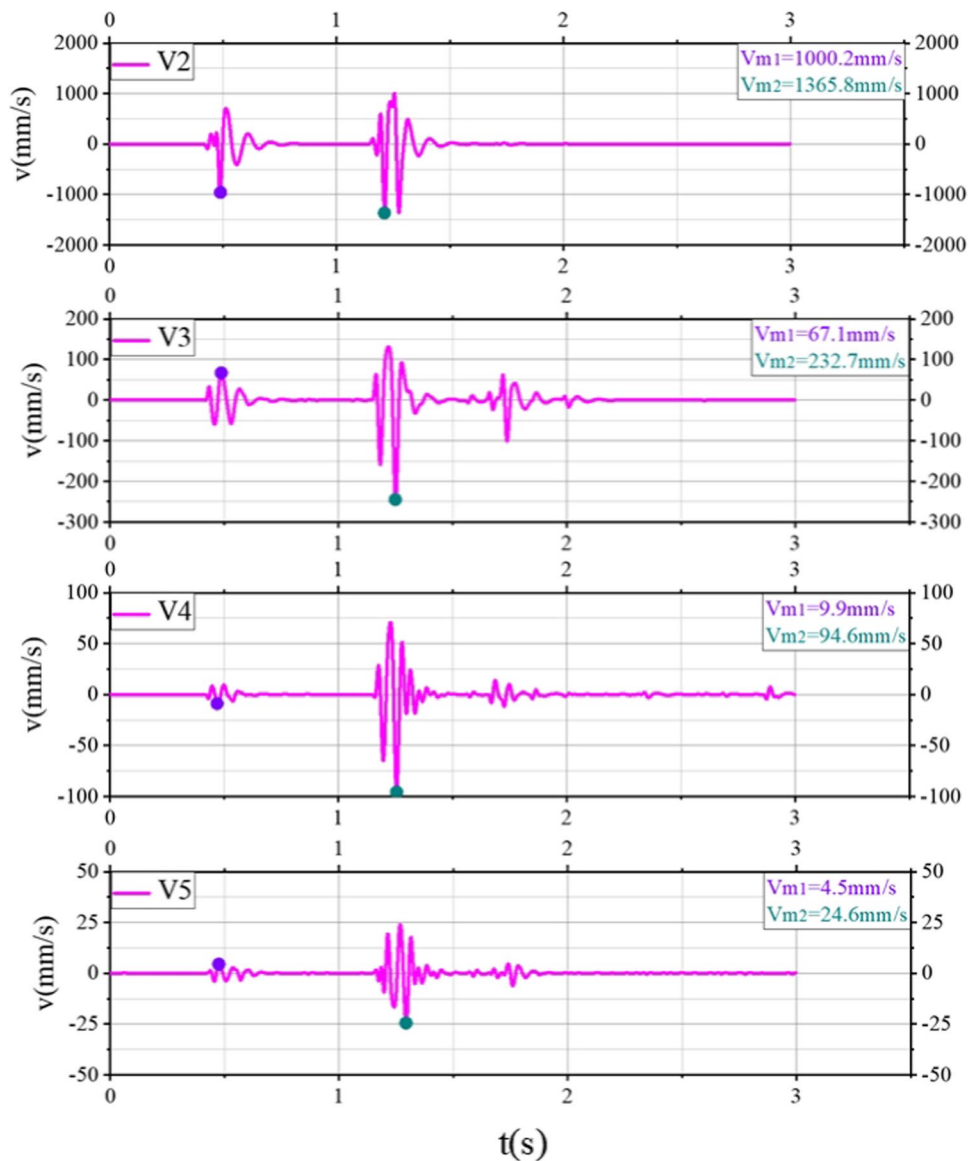
For any signal  $x(t)$ , the Hilbert transform  $y(t)$  is defined as

$$y(t) = \frac{P}{\pi} \int_{-\infty}^{+\infty} \frac{x(\tau)}{t - \tau} d\tau \tag{3}$$

where  $P$  is the Cauchy principal value. After performing the Hilbert transform on each IMF component, the original signal can be written as

$$x(t) = \sum_{j=1}^n a_j(t) \exp\left(i \int \omega_j(t) dt\right) \tag{4}$$

**Fig. 5** Vibration measurement waveform



Therefore, the instantaneous amplitude and frequency can be represented as a function of time in a three-dimensional graph. The frequency-time distribution of the amplitude is called the Hilbert spectrum.

**EMD decomposition of IMF component of vibration signal**

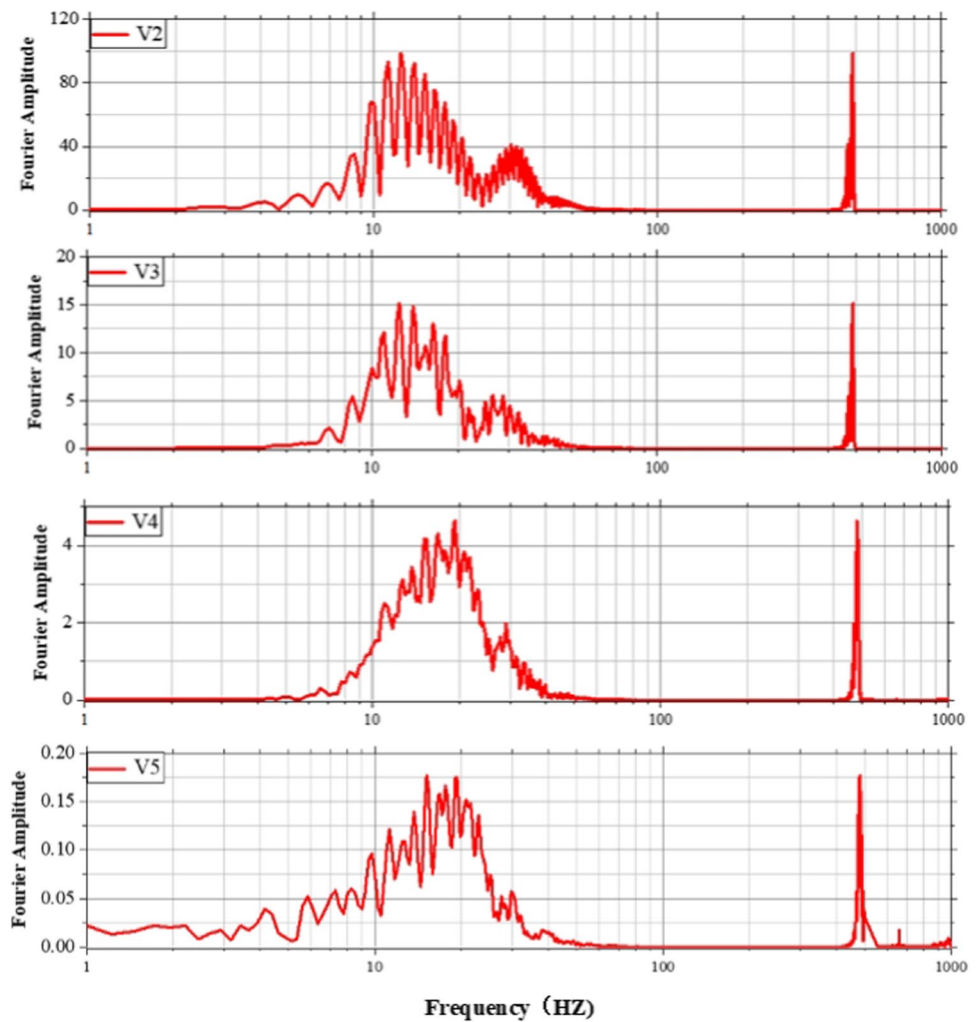
Since there is no a priori basic function, the characteristics of each IMF component are determined by the original waveform, and all IMF components are similar to the original signal. From Fig. 7 we can see that all the waveforms are decomposed into 9–10 IMF components, starting from high frequency to low frequency in turn. Among them, the frequency of the  $c_1$  component is the highest, and the fundamental wavelength is the longest. With the decomposition, the IMF frequency decreases, and the fundamental

wavelength gradually becomes longer until it reaches the last remaining component, which has a very low frequency, and the decomposition is complete.  $c_1$ ,  $c_2$ , and  $c_3$  are the main components of the high-frequency and large-amplitude original signal. These characteristics mean that they contain most of the original energy. As the source distance increases, the energy of high-frequency components ( $c_1$ ,  $c_2$ , and  $c_3$ ) shows an upward trend.

**Hilbert marginal spectrum drawing of Hilbert marginal spectrum mass spectrum waveform**

In Fig. 8, from the edge spectrum, the energy concentration level of the signal in the frequency domain can be obtained, which reveals the law of waveform energy change with frequency. The main frequency band of the dry ice powder

**Fig. 6** Fourier spectrum diagram



pneumatic rock breaking vibration waveform is 0–50 Hz, and some other frequency bands are also included. At the same time, the vibration waveform energy tends to accumulate at low frequencies. The rock mass has a relatively low natural frequency. When the frequency of the IMF component is close to the natural frequency of the rock mass, resonance will occur. The closer the IMFs frequency is to the natural frequency of coal or rock, the more obvious the resonance phenomenon. According to these edge spectra in Fig. 8, we can see that the low-frequency energy of the vibration waveform caused by the aerodynamic rock breaking of dry ice powder occupies the main position. With the increase of the focal distance, the high-frequency energy gradually dominates. The HHT analysis is better than the fast Fourier analysis. The characteristics of the transformation are more obvious.

### Instantaneous energy spectrum

The instantaneous energy spectrum reflects the energy accumulation level of the vibration waveform and the law

of change over time and is the result of the vibration speed and vibration period. The instantaneous energy spectrum of the vibration waveform of each sensor is shown in Fig. 9. It can be seen that the instantaneous energy distribution of the vibration waveform corresponds to the waveform amplitude. Most of the amplitudes of V2 are concentrated at sampling points 1–200 and 500–700. The instantaneous energy is also the same, which corresponds to the excitation of the two fracturing tubes. It can be known that the vibration duration is about 0.4 s. As the focal distance increases, the overall energy level drops, the peak energy of V3 drops to about 7000, and the peak energy of V4 is less than 120. With the increase of the focal distance, the peak value of the fracturing tube of the first shot was lower than that of the fracturing tube of the second shot, and the second shot energy peak value of V4 exceeded that of the first shot.

### Three-dimensional Hilbert spectrum

In order to more clearly express the variation characteristics of the vibration waveform of dry ice powder



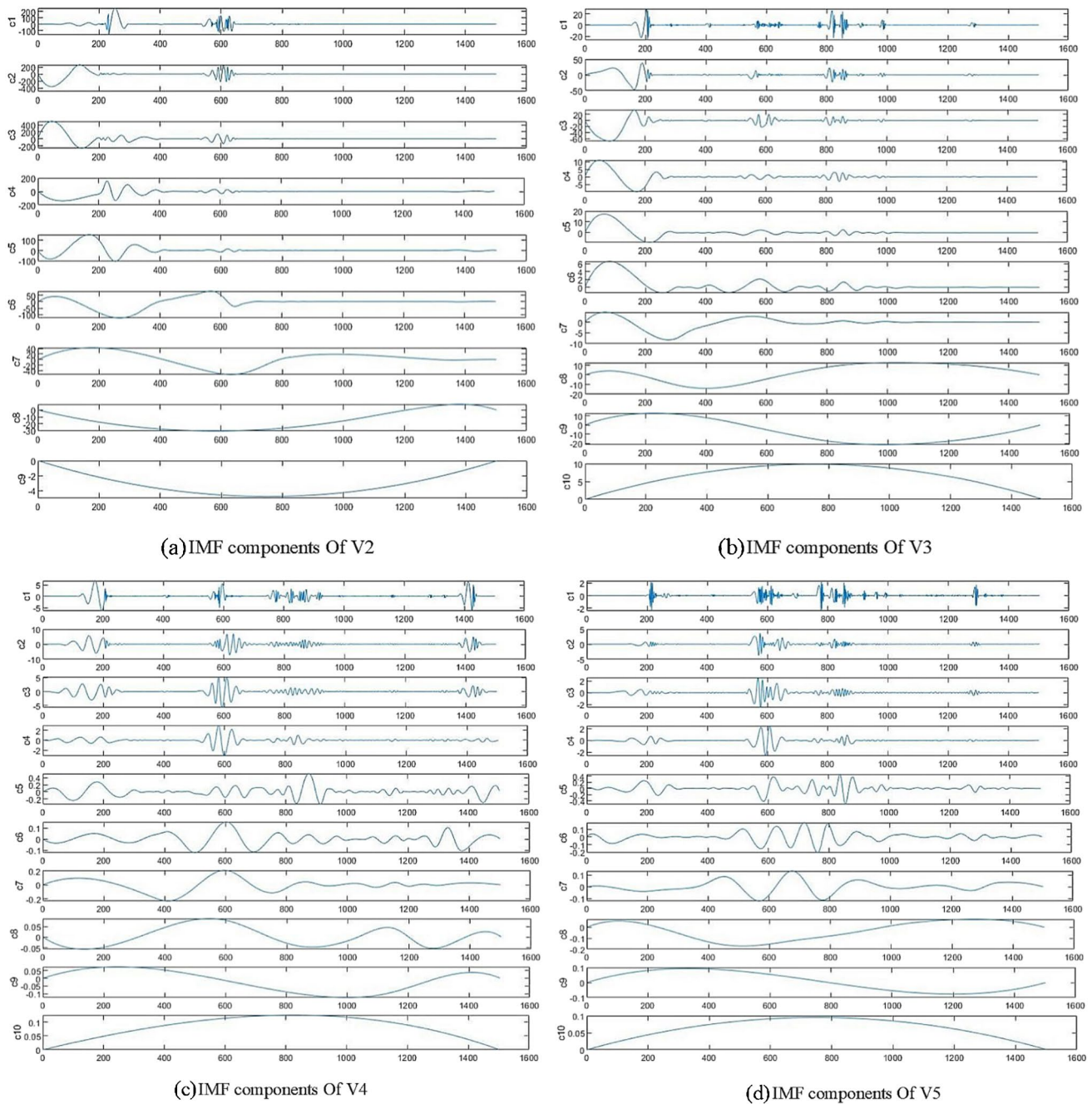


**Fig. 7** IMF components of the vibration waveforms (**a** IMF component of V2 sensor vibration waveform, **b** IMF component of V3 sensor vibration waveform, **c** IMF component of V4 sensor vibration waveform, **d** IMF component of V5 sensor vibration waveform)

pneumatic rock breaking with frequency and time (sampling points), a three-dimensional Hilbert spectrum of the vibration waveform was produced. In Fig. 10, the HHT spectrum is a joint function from the sampling points of V2–V5, the frequency on the horizontal axis, and the energy of the vibration waveform time history on the vertical axis. These parameters are represented in the figure by the color bars on the right side of each image. Energy is

a normalized parameter, indicating the possibility of the existence of a vibration waveform at a certain frequency and time. Vibration signals are composed of components of different frequencies generated by rock fractures. The energy distribution is discrete rather than continuous in a certain frequency range, and there is more than one energy peak. When there is no energy, the energy spectrum is zero. Compared with the Fourier transform, HHT does not

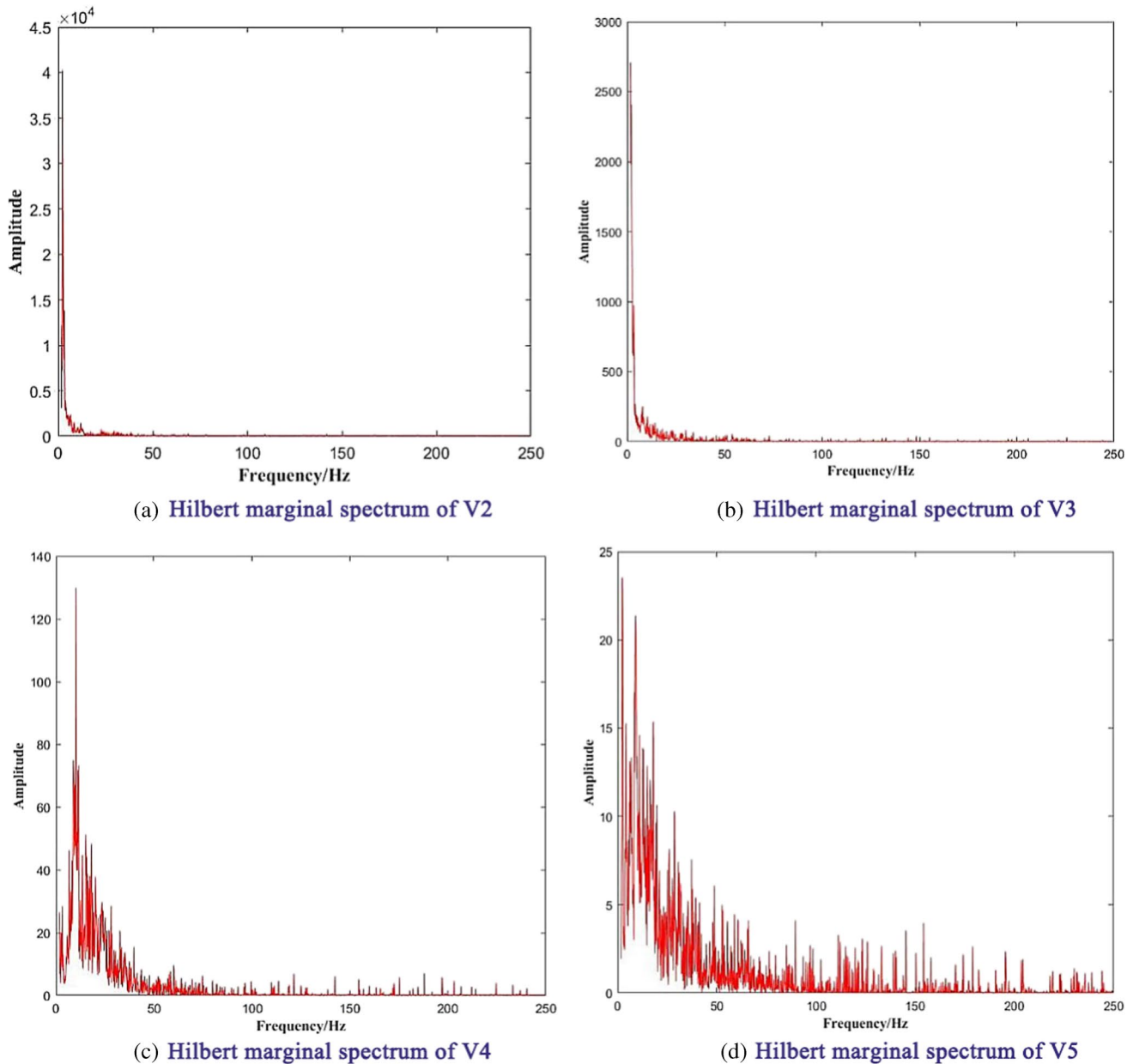


**Fig. 8** Hilbert marginal amplitude spectra (a Hilbert spectrum of vibration waveform of V2 sensor, b Hilbert spectrum of vibration waveform of V3 sensor, c Hilbert spectrum of vibration waveform of V4 sensor, d Hilbert spectrum of vibration waveform of V5 sensor)

cause energy leakage due to the increase of the window and forms a continuous spatial spectral value distribution. Figure 10 shows that the vibration waveform energy is concentrated at sampling points 1–200 and 500–700. As the focal distance increases, the energy distribution in frequency gradually becomes dispersed. The energy distribution of V2 is 0–50 Hz, and the energy distribution of V4 and V5 is more dispersed, and both are distributed between 0 and 150 Hz. The three-dimensional Hilbert spectrum more clearly shows the dynamic change characteristics of the vibration waveform and reflects the phase

characteristics of the waveform. Each phase has its own frequency and energy characteristics.

## Discussion

### Gas wedge in the rock breaking process

At present, the combined action theory of blasting stress wave and blasting gas has been accepted by most researchers because it comprehensively considers the effect of blasting

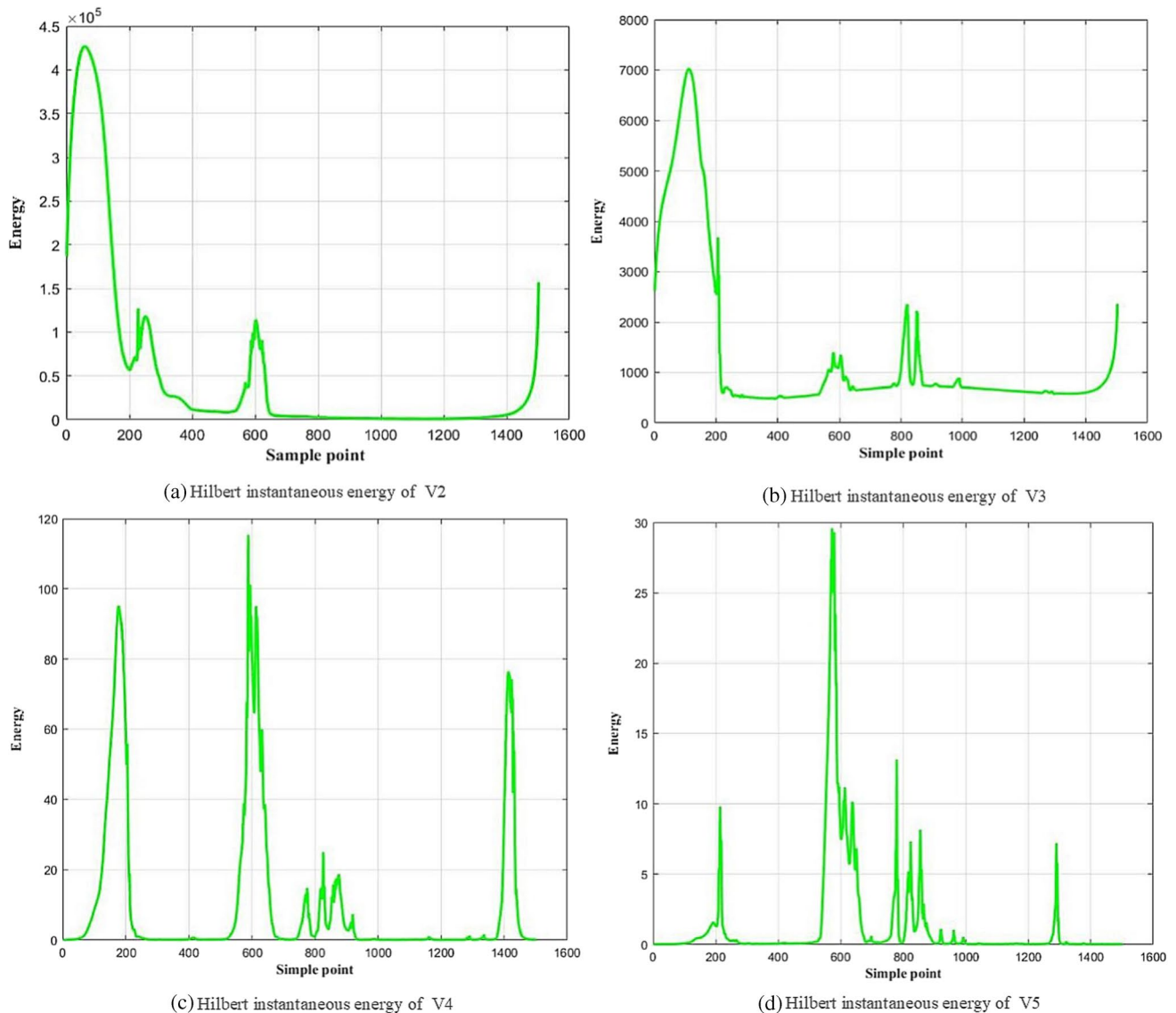


**Fig. 9** Hilbert instantaneous energy (a V2 sensor vibration waveform energy spectrum, b V3 sensor vibration waveform energy spectrum, c V4 sensor vibration waveform energy spectrum, d V5 sensor vibration waveform energy spectrum)

stress wave and blasting gas in the process of rock destruction. The stress wave and blasting gas are viewed from the characteristics of explosion-induced action (Zhu et al. 2008). The combined action theory believes that the stress wave caused by blasting is a dynamic action and is considered to be the main initiator of rock fracture. The effect of blasting gas is considered to be a quasi-static effect, which further enlarges some cracks formed by the stress wave caused by blasting. Using this theoretical basis, the researchers hope to quantitatively analyze the rock destruction effects of the stress wave and blasting gas caused by blasting, and further enrich the rock blasting theory (Li et al. 2006).

According to the theory of combined action of blasting stress wave and blasting gas, rock blasting fracture is divided

into three stages: the first stage corresponds to the process of impact pressure acting on the center of rock blasting to produce initial cracks and decay outward into stress waves. It belongs to the process of dynamic rock breaking; the second stage corresponds to the process in which the stress wave meets the free gate to reflect, and it also belongs to the process of dynamic rock breaking; the third stage corresponds to the stretching caused by high-energy  $\text{CO}_2$  fluid fractured rock and impact pressure. The process of stress coupling propagation of radial cracks is a quasi-static rock breaking process at this stage. In the blasting of traditional explosives, most of the energy is consumed in the form of shock waves within a range of twice the radius of the blast hole from the blast hole. In this range, a rock crushing zone is formed, which is combined

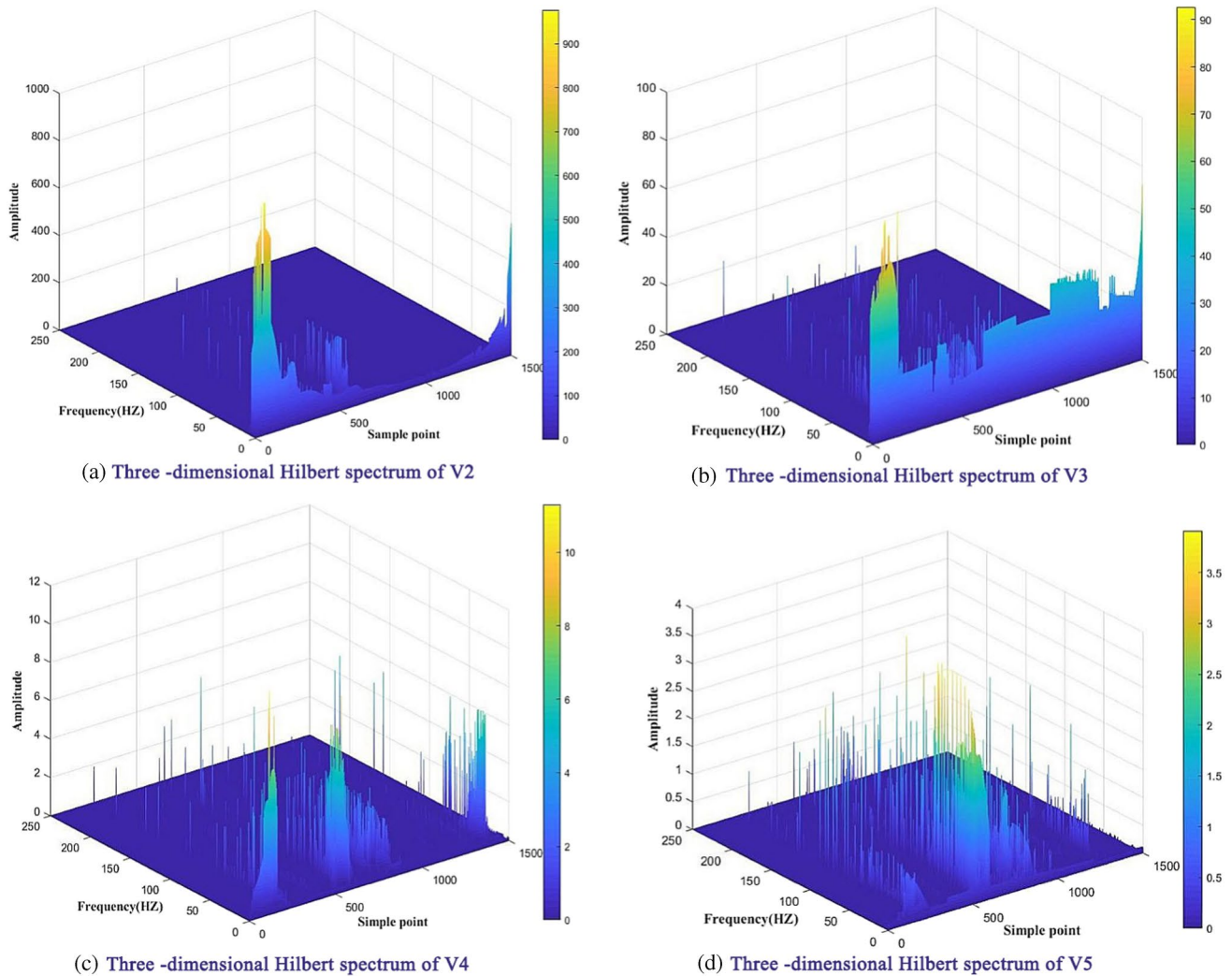


**Fig. 10** Three-dimensional Hilbert spectra **(a)** Three-dimensional Hilbert spectrum of V2 sensor vibration waveform, **(b)** Three-dimensional Hilbert spectrum of V3 sensor vibration waveform, **(c)** Three-dimen-

sional Hilbert spectrum of V4 sensor vibration waveform, **(d)** Three-dimensional Hilbert spectrum of V5 sensor vibration waveform)

with the stress wave and blasting gas. Due to the large rock breaking range and the relatively broken rock, the frequency spectrum distribution of the vibration waveform induced by explosive rock breaking is more complicated than that of dry ice breaking rock. Pneumatic rock breaking by dry ice powder can be divided into two stages. One is the impact of high-pressure  $\text{CO}_2$  gas on the hole wall to generate stress waves, causing microcracks to form around the hole wall; the other is the impact fissures and primary fissures continue to expand and extend under the quasi-static pressure of high-pressure  $\text{CO}_2$  gas expansion. In terms of time, the action time of the first stage is very short, and the action time of the second stage is longer, and the quasi-static effect of high-pressure  $\text{CO}_2$  is the main cause of rock fracture. It can be seen from Fig. 11 that the pneumatic breaking of dry ice powder produced radial main fractures, rock mass uplifting, and rock fragments. The

radial main fissures and rock mass uplifting were caused by the gas wedge, while the rock masses near the boreholes were broken. Due to shock wave reflection, the range of action is small.

### Comparison of HHT and FFT

When analyzing the vibration waveform of dry ice powder pneumatic rock breaking, FFT can only reflect the frequency characteristics of the vibration waveform in the entire frequency domain. In fact, the vibration waveform is time-varying and non-stationary. If we can understand its local characteristics in the time and frequency domains, it is very beneficial to the analysis of vibration waveforms. The time resolution and frequency resolution cannot be arbitrarily small at the same time. HHT can describe waveform

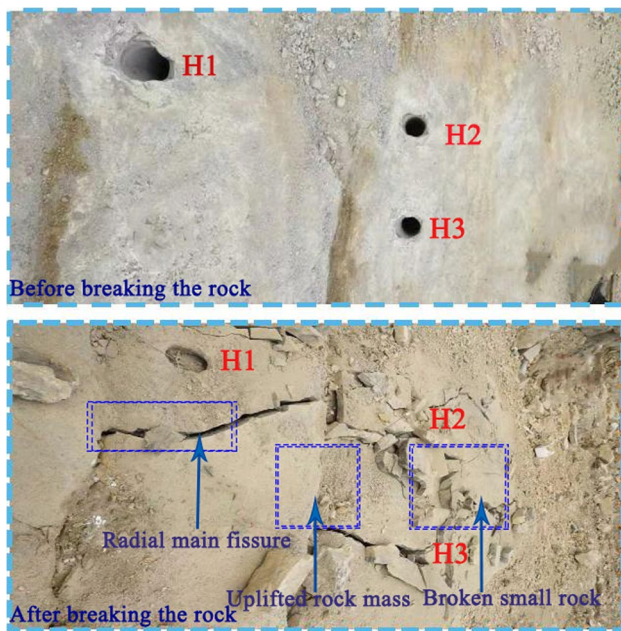


Fig. 11 Comparison of before and after rock breaking

characteristics well in the frequency domain, through which it can estimate the time-varying fundamental frequency spontaneously and can provide accurate time resolution for the energy-frequency representation of the waveform. Empirical mode decomposition does not require a priori basic functions, and IMF components can be obtained through interpolation, so it is more suitable for analyzing waveforms in the frequency domain. In addition, the IMF components decomposed at different time scales can reflect the inherent characteristics of the original waveform. It can be seen from Fig. 7 that most of the energy is concentrated in the  $c_1$ ,  $c_2$ , and  $c_3$  components, and the fundamental wavelength is longer than the other components. In contrast, a basic function is required before FFT, and different basic functions lead to different decomposition results. In addition, the FFT can also cause frequency diffusion and energy loss. The Hilbert edge spectrum statistically shows the cumulative amplitude, which means the possibility of the signal in the frequency domain. Compared with the Fourier transform, the frequency range of the Hilbert marginal spectrum is more accurate. Through the HHT instantaneous energy spectrum, you can clearly see the change law of the waveform energy over time, and the FFT cannot accurately obtain the characteristics of the energy change over time. The three-dimensional Hilbert spectrum (Fig. 10) refers to the non-linear characteristics and correlations of the IMF components of the sample points, frequencies, and energy. These characteristics cannot be obtained by FFT. In addition, HHT will not increase the window, leading to energy leakage and false information. A vibration waveform analysis

technique based on Hilbert-Huang transform in the process of pneumatic rock breaking with dry ice powder is proposed; our results prove the successful application of this technology. The Hilbert-Huang transform obtains the Hilbert spectrum by decomposing the waveform into different IMF components, which provides an effective method for interpreting non-stationary vibration waveforms. The energy of the IMF component is analyzed by the complete waveform, not just the amplitude and energy. Due to the adaptive characteristics of HHT, HHT is superior to the FFT vibration analysis method in processing vibration waveforms.

### Time–frequency distribution analysis and safety evaluation of dry ice powder pneumatic rock breaking vibration energy

Use HHT analysis to observe the distribution characteristics of vibration energy in time and frequency. Observing Fig. 9 shows that vibration energy is mainly distributed at sampling points 1–200 and 500–700. Since the sampling frequency is 500 Hz, it can be seen that the vibration duration is about 0.4 s. According to the sampling point of the interval between two energy fluctuations of 300, it can be seen that the interval between the aerodynamic rock breaking of the two fracturing tubes is 0.6 s. The interval time of pneumatic rock breaking can be obtained by the starting interval of signal energy fluctuation, which provides a reference for the study of the delayed excitation of dry ice powder pneumatic rock breaking. According to Fig. 10, the energy distribution in time and frequency can be comprehensively analyzed. The focal distance of V2 and V3 is less than 7 m. From the perspective of the three-dimensional Hilbert spectrum, their main energy is distributed in 0–50 Hz, and the main part is below 10 Hz. While the focal distance of V4 and V5 is greater than 7 m, their energy distribution in frequency is more dispersed, and the main energy distribution frequency rises. When the focal distance is small, the energy accumulates to the low-frequency band. When the low-frequency and high-energy vibration waveforms accumulate near the rock resonance frequency, the resonance amplification effect will occur, which will increase the instability of the rock and facilitate the fracture of the rock (Bray et al. 1998). However, low-frequency energy also causes more serious damage to buildings. In the safety assessment, not only the maximum vibration wave speed must be considered, but also the frequency distribution of vibration energy must be considered. The test results show that although the maximum vibration wave velocity drops below 25 mm/s when the focal distance is 11 m, the more harmful low-frequency energy has been dispersed to high frequencies when the focal distance is 7 m. It can be seen that the safe distance of dry ice powder pneumatic rock breaking technology is less than 11 m, which is very suitable for rock breaking in complex and sensitive areas in cities.

## Conclusion

In this paper, the Hilbert-Huang transform is used to study the time–frequency energy characteristics of the vibration waveform of dry ice powder aerodynamic rock breaking. Some important conclusions can be drawn from the analysis results:

1. Dry ice powder pneumatic rock breaking technology causes less noise pollution. When the sound source distance is 11 m, the sound pressure level drops to about 100 dB. Compared with the drilling and blasting method, the noise pollution to the surroundings is smaller. It is suitable for urban or other cities. Working in environmentally sensitive areas
2. Compared with FFT, HHT transform is a better tool for extracting the characteristics of blasting vibration waveform. This study shows that the HHT transformation is a relatively simple method to achieve, which can effectively obtain the frequency and energy characteristics of the dry ice aerodynamic rock breaking vibration waveform
3. The HHT three-dimensional Hilbert spectrum shows that when the focal distance is 7 m, the energy distribution in frequency is scattered, and the main energy distribution tends to high frequency, which is beneficial to the protection of surrounding buildings.

This research is helpful to improve the vibration waveform analysis technology and has done basic research for improving the measurement of dry ice aerodynamic rock breaking vibration. In the future, the research direction will be to obtain more on-site vibration data, based on the HHT time–frequency analysis technology, to propose a comprehensive safety evaluation index that also considers the maximum vibration speed, vibration duration, and vibration energy frequency distribution. In the future, the dry ice powder pneumatic rock breaking technology needs more field tests and experimental studies to explain the cracking mechanism of dry ice powder pneumatic rock breaking and the vibration safety assessment of on-site construction. The mechanization and intelligence of dry ice powder pneumatic rock breaking equipment needs to be considered, and more monitoring methods should be added to build the foundation of smart construction sites.

**Funding** This work is supported by the Key Program of National Natural Science Foundation of China (51934007), the Major Scientific and Technological Innovation Program in Shandong Province (2019JZZY020505), the Project Funded by the Priority Academic Program Development of Jiangsu Higher Education Institutions (PAPD), the State Key Laboratory Open Fund (HKLBEF202004) and a Natural Science Foundation of Jiangsu Province (BK20201313).

## Declarations

**Conflict of interest** The authors declare that they have no competing interests.

## References

- Babu TR, Srikanth S, Sekhar AS (2008) Hilbert-Huang transform for detection and monitoring of crack in a transient rotor. *Mech Syst Signal Process* 22(4):905–914
- Benson PM, Vinciguerra S, Meredith PG et al. (2010) Spatio-temporal evolution of volcano seismicity: a laboratory study. *Earth Planet Sci Lett* 297 (8):315–323
- Bray JD, Rathje E, Augello AJ, Merry SM (1998) Simplified seismic design procedure for geosynthetic-lined, solid-waste landfills. *Geosynth Int* 5 (1):203–235
- Chaparro L (2015) Frequency analysis: the Fourier transform (Chapter 5), *Signals and Systems Using MATLAB*, second ed., pp. 333–396.
- Chen HD, Wang ZF, Qi LL (2017) An FH effect of liquid carbon dioxide phase change fracturing technology on gas drainage. *Arab J Geosci* 10:314
- Chernov YK, Sokolov VY (1999) Correlation of seismic intensity with Fourier acceleration spectra. *Phys Chem Earth (A)* 24 (6):523–528
- Chui CK (1992) *An introduction to wavelets*. Academic Press, Inc, New York
- Cohen L, Bai JX (1998) *Time–frequency analysis theory and application*, Xi an Jiaotong University Press.
- Dhanya J, Gade M, Raghukanth STG (2017) Ground motion estimation during 25th April 2015 Nepal earthquake. *Acta Geod Geoph* 52(1):69–93
- DOBRTZ B M, CRAWFORD P, C.LLNL (1985) *explosives handbook: properties of chemical explosives and explosive stimulants* [M]. [S. 1.]: Lawrence Livermore National Laboratory
- Donze FV, Bouchez J, Magnier SA (1997) Modeling fractures in rock blasting. *Int J Rock Mech Min Sci* 34(8):1153–1163
- Ebrahim F, Salm, Ewan J. Sellers (2021) A review of the methods to incorporate the geological and geotechnical characteristics of rock masses in blastability assessments for selective blast design. *Eng Geol* 281:105970
- Elgamel SA, Soraghan J (2011) Empirical mode decomposition based multipulse processor for enhanced radar tracking in the presence of high-power interference. *LET Radar Sonar Navigat* 7:769–779
- Feng Zheng-Yi, Yen-Rou Lu (2021) A numerical simulation of seismic signals of coseismic landslides. *Eng Geol* 289:106191
- Gao F, Tang L, Zhou K, et al. (2018) Mechanism analysis of liquid carbon dioxide phase transition for fracturing rock masses [J]. *Energies*, 11(11)
- Global J (1995) Cardox system brings benefits in the mining of large coal. *Coal International* 243:27–28
- Goodarzi M, Mohammadi S, Jafari A (2015) Numerical analysis of rock fracturing by gas pressure using the extended finite element method. *Pet Sci* 12:304–315
- Haugen S. (2018) *Rock fragmentation in mining-past, present and future*[C]// 12th International Symposium on Rock Fragmentation by Blasting, Lule, Sweden, 34–37
- He MC, Miao JL, Feng JL (2010) Rock burst process of limestone and its acoustic emission characteristics under true-triaxial unloading conditions. *Int J Rock Mech Min Sci* 47(11):286–298

- Hu SB, Pang SG, Yan ZY (2019) A new dynamic fracturing method: deflagration fracturing technology with carbon dioxide. *Int J Fract* 220:99–111
- Kaveh A, Bakhshpoori T, Hamze-Ziabari SM (2016) Derivation of new equations for prediction of principal ground-motion parameters using M5 algorithm. *J Earthquake Eng* 20(6):910–930
- Kumar S, & Mishra AK (2020) Reduction of blast-induced ground vibration and utilization of explosive energy using low-density explosives for environmentally sensitive areas. *Arabian J Geosci* 13(14). <https://doi.org/10.1007/s12517-020-05645-8>
- Kutter HK and Fairhurst C (1971) On the fracture process in blasting. *Int J Rock Mech Mining Sci Geomechanics Abstracts* 8(3): 181IN1, 189–188, IN10, 202.
- Li XL, Li ZH, Wang EY et al (2016a) Analysis of natural mineral earthquake and blast based on Hilbert-Huang transform (HHT). *J Appl Geophys* 128(5):79–86
- Li XL, Li ZH, Wang EY et al (2016b) Extraction of microseismic waveforms characteristics prior to rock burst using Hilbert-Huang transform. *Measurement* 91:101–113
- Li Q et al (2018) Application of liquid CO<sub>2</sub> phase change rock breaking technology in subway foundation pit excavation. *J Railway Sci Eng* 15(1):163–169
- Li N, Chen LJ, Zhang P (2006) Dynamic analysis for fracturing progress by detonation gas. *Chin J Geotech Eng.*;28(4):460–463 [in Chinese]
- Li Qi-Yue, Chen Guan, Luo Da-You, Ma Hai-Peng, Liu Yong. (2020) An experimental study of a novel liquid carbon dioxide rock-breaking technology. *Int J Rock Mech Mining Sci* 128:104244
- Liu Xiaoxiong, et al. (2018) Study on vibrational energy distribution of rock-solid phase change in liquid carbon dioxide. *Mining and metallurgy engineering*, Vol. 38, Issues 181(3), p. 5–10
- Lu CP, Dou LM, Zhang N et al (2013) Microseismic frequency-spectrum evolutionary rule of rockburst triggered by roof fall. *Int J Rock Mech Min Sci* 64(12):6–16
- Lu CP, Dou LM, Liu B, et al. (2012) Microseismic low-frequency precursor effect of bursting failure of coal and rock. *J Appl Geophys* 79 (4)55–63
- Ma et al (2018) Qualitative method and case study for ground vibration of tunnels induced by fault-slip in underground mine. *Rock Mech Rock Eng.* <https://doi.org/10.1007/s00603-018-1631-x>
- Ma et al (2019) Ground motions induced by mining seismic events with different focal mechanisms. *Int Rock Mech Min Sci* 116:99–110
- Mallat S (1989) A theory for multiresolution signal decomposition: the wavelet representation, *IEEE Trans. Pattern Anal Mach Intell* 11 (7)674–793
- Mondal Debjeet, Roy PNS (2019) Fractal and seismic b-value study during dynamic roof displacements (roof fall and surface blasting) for enhancing safety in the longwall coal mines. *Eng Geol* 253:184–204
- Morlet J (1982) Wave propagation and sampling theory, *Geophysics* 47(2)203–236
- Nilson RH, Proffer WJ, Duff RE (1985) Modelling of gas-driven fractures induced by propellant combustion within a borehole. *Int J Rock Mech Mining Sci Geomech Abstracts* 22(1):3–19
- Rachel EL, Willsky AS (1995) A wavelet packet approach to transient signal classification. *Appl Comput Harm Anal* 2(3):265–278
- Roy MP, Mishra AK, Agrawal H, & Singh PK (2020) Blast vibration dependence on total explosives weight in open-pit blasting. *Arab J Geosci* 13(13). <https://doi.org/10.1007/s12517-020-05560-y>
- SANCHIDRIÁN J A.SLIM (2018) Technology for blasting to improve mining[C]12th International Symposium on Rock Fragmentation by Blasting,Lule a,Sweden.
- Singh, C. P., Agrawal, H., & Mishra, A. K. 2020, A study on influence of blast-induced ground vibration in dragline bench blasting using signature hole analysis. *Arabian Journal of Geosciences*, 13(13). <https://doi.org/10.1007/s12517-020-05562-w>.
- Skeberis C, Zaharis ZD, Xenos TD et al (2015) Time-frequency analysis of VLF for seismic-ionospheric precursor detection: evaluation of Zhao–Atlas–Marks and Hilbert–Huang transforms. *Phys Chem Earth* 2:1–11
- Song DZ, Wang EY, Li ZH et al (2015) Energy dissipation of coal and rock during damage and failure process based on EMR. *Int J Min Sci Technol* 25(5):787–796
- Song Danqing, Zhuo Chen (2020) Seismic response analysis of a bedding rock slope based on the time-frequency joint analysis method: a case study from the middle reach of the Jinsha River, China. *Eng Geol*
- Wang X, & Cai M (2017). Numerical analysis of ground motion in a South African mine using SPECSEM3D. In *Proceedings of the First International Conference on Underground Mining Technology* (pp. 255–268). Australian Centre for Geomechanics.
- Wu Z.H, Huang NE (2004) A study of the characteristics of white noise using the empirical mode decomposition method. (*Proc. Royal. Soc. London Ser. A*)*Proceedings of the Royal Society A-Mathematical Physical and Engineering Sciences* 460 1597–1611
- Xie Xiaofeng, et al. (2018) Review of liquid CO<sub>2</sub> phase transformation rock breaking technology. *J Railway Sci Eng* 15(6)
- Yang .Z.G, R.C. Yu, R. Guo, et al. (2008) Application of microseismic monitoring to deep mines, *Chin. J Rock MechEng* 27(5):1066–1073
- Yang Xiaofeng, Li Yanhong, Nie Aiguo, Zhi Sheng and Liu Liyuan (2020) Numerical study on rock breaking mechanism of supercritical CO<sub>2</sub> jet based on smoothed particle hydrodynamics. *Comput Model Eng Sci* 1–17
- Yingguo Hu, Wenbo Lu (2018) Numerical and experimental investigationDerivation of new equations for prediction ofon of blasting damage control of a high rock slope in a deep valley. *Eng Geol* 237:12–20
- Zhang YA, Deng JR, Deng HW, Ke B (2019) Peridynamics simulation of rock fracturing under liquid carbon dioxide blasting. *Int J Damage Mech* 28:1038–1052
- Zhang Guo-Hua, Wu Chen (2020) A failure probability evaluation method for collapse of drill-and-blast tunnels based on multistate fuzzy Bayesian network. *Eng Geol* 276:105752
- Zhang Y, Deng J, Deng H, et al. (2018) Peridynamics simulation of rock fracturing under liquid carbon dioxide blasting[J]. *Int J Damage Mech*
- Shengtao Z Nan J, He Xu, Xuedong L (2020) Rock breaking and dynamic response characteristics of carbon dioxide phase transition fracturing considering the gathering energy effect. *Energies* 1336. <https://doi.org/10.3390/en13061336>
- Zhu ZM, Xie HP, Mohanty B (2008) Numerical investigation of blasting-induced damage in cylindrical rocks. *Int J Rock Mech Min Sci* 45(2):111–121